BRAHMS experimental results obtained in d-Au collisions at $\sqrt{s_{NN}} = 200$ GeV

Abstract. During the 2003 run d-Au collisions at 200 AGeV have been investigated at Relativistic Heavy Ion Collider (RHIC) from Brookhaven National Laboratory (BNL), U.S.A. Using the BRAHMS Experiment detectors interesting results on charged particle multiplicities, rapidity distributions, transverse momentum spectra, antiparticle to particle ratios and participant region evolution have been obtained. Taking into account the importance of the collision geometry in the investigation of the collision mechanisms, the most interesting experimental results are presented for different rapidity and collision centrality ranges. Comparisons with similar experimental results obtained in Au-Au collisions for evidencing the importance of the collision geometry on the collision dynamics are done, too. The most significant results are related to the evolution of the nuclear modification factor, with the rapidity and collision centrality, the high transverse momentum suppression and the behaviours in different rapidity and centrality ranges. They could suggest strong initial state effects. These effects could be related to the gluonic structure of the colliding nuclei. Some connections with the Colour Glass Condensate formation are possible.

1. Introduction

The BRAHMS (**B** road **R** Ange **H** adron **M** agnetic **S** pectrometers) Experiment is placed at two o'clock on the ring of the **R** elativistic **H** eavy **I** on **C** ollider (RHIC) from Brookhaven National Laboratory (USA). This experimental set-up was designed to gather information on the interesting physical quantities characterising various emitted particles in ultrarelativistic nuclear collisions as functions of transverse momentum, p_T, and rapidity, y [1–6].

The yields as function of rapidity offer information on the nuclear density into a

given collision, as well as on the produced entropy. The information on the collision dynamics and the thermalisation degree is obtained from the spectral shapes of the interesting physical quantities and their dependencies on rapidity. Important information on the collision dynamics is obtained from collision centrality measurements, and the information from the times in the reaction is included in the high pT parts of the spectra. Therefore, important information on the collision dynamics and its connections with collision geometry can be obtained.

In the four running years many experimental data have been collected in Au-Au collisions at $\sqrt{s_{NN}} = 62.4 GeV$, $\sqrt{s_{NN}} = 130 GeV$ and $\sqrt{s_{NN}} = 200 GeV$, as well as in d-Au collisions at $\sqrt{s_{NN}} = 200 GeV$. The experimental data obtained in p-p collisions at the same energies are used as reference data.

The main motivations for d-Au collisions are related to the possibility to consider as references for high transverse momentum suppression observed in Au-Au collisions at RHIC-BNL energies, as well as, survey at large rapidities.

The experimental results include information on charged particle multiplicity, pseudorapidity and rapidity distributions, participants, energy density, nuclear temperatures and radial flow, antiparticle to particle ratios, Coulomb momentum, chemical potentials, entropy per baryon and high p_T suppression. All quantities offer information on the behaviour of the highly excited and dense nuclear matter formed in the overlapping region of the two colliding nuclei, as well as on the possible formation of some new forms of the nuclear matter. Some comments and comparisons with different assumptions are included, too.

The experimental results are presented for different rapidity or pseudorapidity values, situated in the range from $\eta \approx -4.2$ up to $\eta \approx 4.2$. Four cuts in collision centrality are considered, namely: 0-30%, 30-60%, 60-80%, as well as, minimum bias.

Before the presentation of the experimental results, a short description of the unique capabilities of the BRAHMS detector system for precise momentum determination and particle identification is done.

2. The BRAHMS experimental set-up

In the BRAHMS Experiment two different regimes can be studied, namely: (i) a baryon poor region with a high energy density, created at mid-rapidity; (ii) a region near the initial nuclei, at high rapidities, very rich in baryons at relatively high temperature. Therefore, in the BRAHMS experiment, well identified charged hadrons - $\pi^{\pm}, K^{\pm}$, p, $\bar{p}$ - over a wide range of rapidity and transverse momenta at all energies and beams available at RHIC can be measured. These two regimes can offer interesting dynamics information.

Taking into account the accelerator system structure and the size of the experimental halls the BRAHMS spectrometers are small solid angle devices. They provide semi-inclusive measurements in very different eexperimental conditions.

TThe experimental set-up was designed with two moveable magnetic spectrom-

eters, namely: (a) **F** orward **S** pectrometer (FS); (b) **M** id **R** apidity **S** pectrometer (MRS) [1–5]. The Forward Spectrometer covers the angular region $2.3\circ \leq \theta \leq 30\circ$, and the Mid Rapidity Spectrometer covers the angular region $30\circ \leq \theta \leq 95\circ$. The pseudorapidity ranges covered by the two spectrometers are: $1.3 \leq \eta \leq 4.0$, $-0.1 \leq \eta \leq 1.3$, respectively. To the two magnetic spectrometers three event characterization detector systems have been added; they provide global information. The three detectors systems are the following: **B** eam-**B** eam **C** ounters (BBC), multiplicity detector and **Z** ero **D** egree **C** alorimeters (ZDC). Together, the three detector systems will provide centrality coverage in the mid rapidity region, namely: $-2.2 \leq \eta \leq 2.2$, in the region $3.2 \leq |\eta| \leq 4.3$, as well as at 0^0. A top view of the BRAHMS experimental set-up is shown in Fig.1.

The Forward Spectrometer is unique in the family of RHIC-BNL experiments in that it can identify hadrons up to the rapidity $y \approx 4$. It covers a large momentum and transverse momentum range.

The Mid-Rapidity Spectrometer has a large angular coverage. Together with the **P** article **I** dentification (PID) the Mid-Rapidity Spectrometer extends and complements measurements by the other RHIC detectors and provides comparisons between mid-rapidity and forward rapidity spectra with the same experimental set-up. Despite the small solid angles of the spectrometers, the transverse momentum spectra of identified particles can be measured up to $p_T \approx 4$ GeV/c with a readily obtainable integrated luminosity.

The experimental data for d-Au collisions at $\sqrt{s_{NN}} = 200 GeV$ have been collected with the both spectrometers, as well with the new added INEL detectors because of the low multiplicity of the very asymmetric nucleus-nucleus collisions. The INEL detectors as used as trigger in minimum bias events. As was mentioned previously, it increased the coverage in pseudorapidities up to 5.29. Using this new trigger almost (913)% from the d-Au inelastic collisions can be selected. Almost (715)% from the total inelastic processes in p-p collisions is selected, too. The cross sections for the mentioned processes are 2.4 b and 41 mb, respectively.

Therefore, the Physics topics that BRAHMS Collaboration addresses are related to these opportunities, namely: study of the hot and dense system formed in heavy ion collisions in a systematic way as function of system size, collision energy, centrality and rapidity [1–6]. The present work tries to present a step from this general effort.

3. Particle identification and momentum determination

Particle identification can be done using different ways. First of all, the detectors from the two spectrometers can be used to combine the time-of-flight measurements in the two hodoscopes (H1 and H2 in Fig.1) with measurements in the threshold Cherenkov counter (C1) and the Ring Imaging Cherenkov Counter (RICH). The 48 scintillator slats in the first hodoscope and the 32 scintillator slats in the second hodoscope - instrumented with photomultiplier tubes (PMT) at each end - allow the
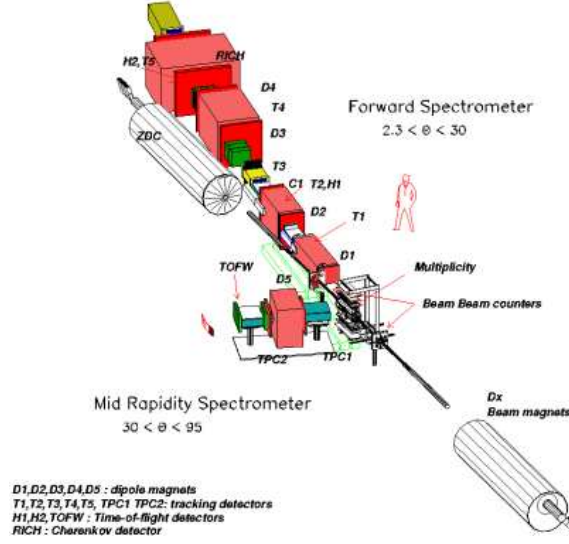
Fig. 1. A top view of the BRAHMS Experiment

particle identification in the momentum range 1-20 GeV/c, in Forward Spectrometer. The time-of-flight array in Forward Spectrometer is place at 8.6 m from the nominal vertex position. Mid Rapidity Spectrometer uses for particle identification two time projection chambers (TPC1 and TPC2), a dipole magnet (D5) and a time-of-flight wall (TOFW) with 83 scintillator slats, placed at 4.3 m from the nominal vertex position. In the two arms of the BRAHMS experimental set-up the overall time resolution is around 120 ps. A second time-of-flight wall was introduced in 2003. In the Forward Spectrometer the separation of kaons and protons is possible in the momentum range $p < 4.5$ GeV/c, and in Mid Rapidity Spectrometer in the momentum range $p < 2.2$ GeV/c.

Another way is related to the momentum spectra and effective mass. In the MRS, pions and kaons could be well separated up to 1.5 GeV/c. For fixed rapidities the m2 spectra for positive and negative particles have been obtained. The following relation has been used:

$$m^2 = p^2(\frac{t^2}{L^2} - 1) \tag{1}$$

where p is the particle momentum, t is the time-of-flight and L is the flight distance.

The particles momenta are determined by projecting the straight-line tracks as reconstructed in the two TPCs to the magnets. After this the bending angle at matched tracks using an effective edge approximation is calculated. For obtaining
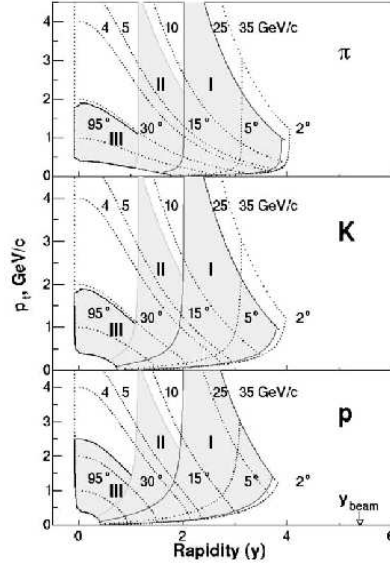
Fig. 2. Acceptance maps for BRAHMS experimental set-up

momentum spectra the vertex dependent acceptance maps have been used. For vertex position is in the range from -15 cm to +15 cm the transverse momentum is in the range from 0.3 GeV/c to 3.0 GeV/c. For the full magnetic field the resolution in momentum was $\delta p/p = 0.0077p$, for the Mid Rapidity Spectrometer. In the same conditions, the momentum resolution for the Forward Spectrometer was $\delta p/p = 0.0018p$[2–5]. This resolution is enough for tracking considerations and spectra measurements.

For particle identification the acceptances for the two spectrometers can be used, too (Fig.2). It is important to stress here that the acceptances for the two spectrometers, at a given field, for positive charged particles, are equal to the acceptances for negative charged particles at the opposite polarity of the given magnetic field. This result is important, also, for the particle ratios.

4. The charged particle multiplicity,pseudorapidity distribution and rapidity distribution in d-Au collisions

The pseudorapidity distribution, as well as the collision centrality dependence of the emitted charged particles densities could be influenced, in relativistic heavy ion collision, by a manifestation of high density QCD, namely: saturation of the initial parton densities [7, 8]. The charged particle pseudorapidity density distributions obtained in Au-Au collisions at $\sqrt{s_{NN}} = 130 GeV$ and $\sqrt{s_{NN}} = 200 GeV$ have been used to constrain model predictions [9–12]. Taking into account that they were

inconclusive about whether parton saturation in the initial state contributes significantly to the reaction dynamics using different assumptions as saturation models or energy loss mechanisms, other collision types were performed. This was imposed by the other model ambiguity, too, namely: suppression of the high transverse momentum of the charged particles in Au-Au collisions. The study of the d-Au collisions at $\sqrt{s_{NN}} = 200 GeV$ could confirm that the global particle yields offer a definitive signature of parton saturation [13].

For obtaining global information the Beam-Beam Counters (BBC), multiplicity detector and Zero Degree Calorimeters (ZDC) have been used. The Beam-Beam Counters provide the initial trigger and vertex information. They assure the start time for the time-of-flight measurements, too. Each of the elements of the BBCs has 3 cm and 4 cm UVT Cherenkov radiator read out by PMTs. The right side of the BBCs consists from 36 elements and the left side consists from 44 elements; they are positioned at $\pm 2.2m$ from the nominal vertex interaction. The BBCs are used to determine the pseudorapidity densities at larger pseudorapidities, too.

The multiplicity detector provides information on the collision centrality. 24 segmented Si-detectors with 168 channels (SiMA = Si Multiplicity Array) and 40 scintillator squared tiles with 12 cm length (TMA = Tiles Multiplicity Array) are included in this hybrid detector. The pseudorapidity range covered by the multiplicity detector is $-2.0 \leq \eta \leq 2.0$. Common devices for all experiments at RHIC are the Zero Degree Calorimeters [5]. At the BRAHMS experiment they are placed at $\pm 18m$ from the nominal vertex interaction, being situated behind the two DX beam-line magnets. For Au-Au collisions the two ZDCs offer information on the collision centrality measuring the forward going spectator neutrons. The coverage provides by the global detectors is in the region $-2.2 \leq \eta \leq 2.2$, in the region $3.2 \leq \mid \eta \mid 4.3$, as well as at 0^0.

In this experiment, for centrality determination, the Si Multiplicity Array (SiMA) and the Scintillator Tile Multiplicity Array (TMA) have been used. They have been used to measure the pseudorapidity densities close to the mid-rapidity. They have been used in the four runs to measure the overall charged particle production and to determine collision centrality. SiMA and TMA can be hit by many different particles, including background particles. Therefore, to obtain the multiplicity information it is necessary to convert the deposited energy into a number of hits. The energy loss signal is transformed to charged particle multiplicity dividing total deposited energy to the expected deposited average energy by one particle in a tile. Conversion factors are evaluated from GEANT simulations. The background contributions are considered. They are between 10% for SiMA elements and 30% for TMA elements. All detector elements were calibrated in energy using pulsers, cosmic rays and sources measurements. It is important to stress that the layout of the SiMA and TMA for the d-Au collisions is similar to that presented for Au-Au collisions at the mentioned energies, for multiplicity analysis.

To increase the number of events for that there is possibility in the vertex determination the "Inelasticity Counters" (INEL) has been developed. It consists of a plastic scintillator ring that is segmented into four pieces and arranged about

the beam pipe. This detector subsystem was developed in connection with the detectors system for pp2pp Experiment [13]. It is used for a close to minimum bias experiment trigger and for providing vertex position information in cases where the beam-beam counter arrays are not able to establish this information. Three pairs of the "Inelasticity Counters" were used to develop a near to minimum bias trigger by detecting charged particles in the pseudorapidity range $3.2 \leq \mid \eta \mid 5.2$. They were placed at ± 155 cm, ± 416 cm, ± 660 cm, respectively, in comparison with the nominal vertex. With the INEL array relative time-of-flight measurements have been performed. They were permitted a resolution of around 5 cm for the interaction vertex determination. The INEL subsystem detector provides the minimum bias trigger for the experiment, too. The counters from the subsystem are sensitive to 913% of the total inelastic cross section. This result is obtained using GEANT simulations.

Collision centrality was determined using a geometry-weighted average of SiMA and TMA multiplicities. The multiplicities obtained with the two detector subsystems are corrected for the distances between the nominal interaction vertex and the actual interaction vertex, specific for each event. Again, the GEANT simulations were been used to correct for the possibility that neither the SiMA nor the TMA detectors will be hit by a particle for the most peripheral events. The normalized SiMA and TMA averaged multiplicities are included in the Fig.3. The results are presented for the following collision centrality ranges: 0-30 %, 30-60 % and 60-80 %. These collision centralities were obtained by integrating the yield under the multiplicity curve. For the centrality range 0-30 % the both nucleons of the deuteron are expected to participate in the collision.

The multiplicity distribution obtained in d-Au collisions at $\sqrt{s_{NN}} = 200 GeV$ is different in comparison with the multiplicity distribution obtained in Au-Au collisions at the same energy. In this case, the extended flat regions, as well as, the well-defined high multiplicity knee are missing. This distribution reflects the smaller number of participant nucleons in d-Au collisions. Therefore, the measurements performed in d-Au collisions are more sensitive to the underlying nucleon-nucleon collision multiplicity distribution.

The charged particle multiplicity determined in d-Au collisions at $\sqrt{s_{NN}} = 200 GeV$ on the whole pseudorapidity range was $N_{ch}^{dAu} = 398 \pm 42$. This value is significantly smaller than the multiplicities obtained previously. Thus, in Au-Au collisions at $\sqrt{s_{NN}} = 130 GeV$ the charged particle multiplicity on the whole pseudorapidity range was $N_{ch}^{130} = 4050 \pm 300$, and for the same collisions, at $\sqrt{s_{NN}} = 200 GeV$ the charged particle multiplicity was $N_{ch}^{200} = 5100 \pm 300$. A consequence of the small particle multiplicities, in different collision centrality ranges, in d-Au collisions at $\sqrt{s_{NN}} = 200 GeV$ is the relatively large range of the fraction of the detected particles for a given total number of emitted particles.

The pseudorapidity distributions, $\frac{dN}{d\eta}$, has been obtained using solid angle evaluations (Fig.4.a,b). In the figure are included charged particles pseudorapidity density plots for minimum-bias events, as well as, 0-30 %, 30-60 % and 60-80 % collision centrality ranges. As in the multiplicity determination, the SiMA and TMA
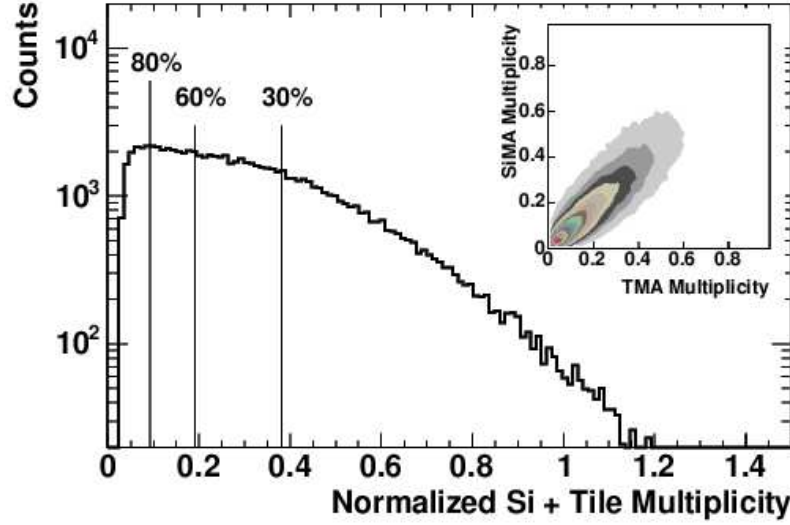
Fig. 3. SiMA and TMA averaged multiplicity distribution. It is normalized to the 1 % centrality level. Efficiency limits for a few centralities are included

detector subsystems results have been averaged. Statistical uncertainties are in the limit of the plotted points. The systematic uncertainties were estimated at 8 % for the two detector subsystems and are shown by horizontal brackets in the plots. For the results obtained using BBCs the systematic uncertainties are around 12 %. All systematic uncertainties are established by exploring the variation of the deduced pseudorapidity densities to reasonable changes in the energy calibrations and background subtraction. The experimental data and their uncertainties obtained in the BRAHMS Experiment are in agreement with others reported [14]. The negative pseudorapidities indicate the gold fragmentation region, and the positive pseudorapidities reflect the deuteron fragmentation region. Differences between the two regions can be observed.

The pseudorapidity distributions, for different centralities have been fitted with different models. In Fig.4.a,b the predictions of the models based on HIJING [15] (solid curves) and AMPT [16] (dashed curves) simulation codes, as well as the predictions of the saturation model [17]. The HIJING simulation code model and the modified saturation model (Fig.5) [18] seem to reproduce the experimental results. The agreement is obtained, in the saturation model, taking into account the experimental number of participants, as well as the possibility to have additional interactions and participants in the gold region, mainly in the rapidity range $-5 \leq y \leq -3$ [18].

It is important to stress again that in Au-Au collisions at the two energies a large plateau for particle production in very central collisions (6%) was obtained in
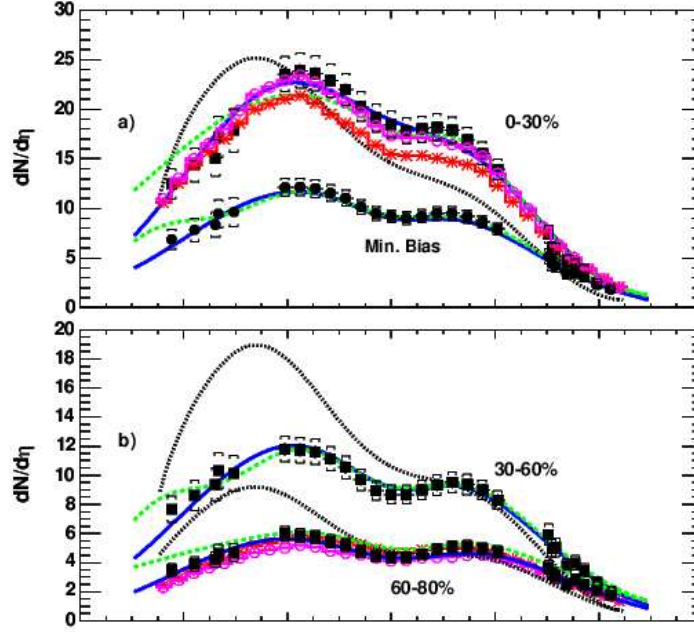
Fig. 4. (a) and (b) Pseudorapidity distribution of the charged particles in d-Au collisions at $\sqrt{s_{NN}} = 200 GeV$ for indicated centrality range. The solid, dashed and dotted curves are the results of the HIJING, AMPT and Saturation models, respectively.
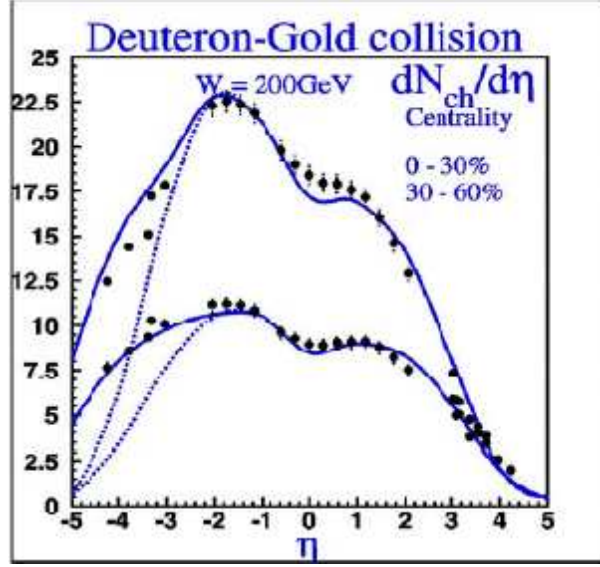
Fig. 5. Comparisons of the charged multiplicity distribution in pseudorapidity for different centrality cuts in d-Au collisions at $\sqrt{s_{NN}} = 200 GeV$ with the predictions of the modified saturation model

the pseudorapidity range $-2.0 \leq \eta \leq 2.0$, including the range ends. This plateau does not appear in d-Au collisions at $\sqrt{s_{NN}} = 200 GeV$. For the most central Au-Au collisions (0-5%), the values obtained from pseudorapidity distributions, at $\eta = 0.0$, were: $\frac{dN}{d\eta}|_{ch}^{130} = 550 \pm 30$, $\frac{dN}{d\eta}|_{ch}^{200} = 610 \pm 50$, respectively. These values are in good agreement with HIJING code predictions [12, 19, 6]. The full widths at the half maximum are: $\Delta\eta_{ch}^{130} = 7.6 \pm 0.7$, $\Delta\eta_{ch}^{200} = 7.9 \pm 1.0$, respectively. In d-Au collisions at $\sqrt{s_{NN}} = 200 GeV$ this value, at $\eta = 0.0$, for the most central collisions (0-30%), is much more smaller, namely: $\frac{dN}{d\eta}|_{ch}^{dAu200} = 18.5 \pm 0.5$[13]. Taking into account the two fragmentation regions, for deuteron and gold, respectively, the value of the pseudorapidity density in the gold region (≈ 23.5) is higher than the corresponding value in the deuteron region (≈ 17.5).

The rapidity or pseudorapidity distribution can be used to estimate energy densities at the meson production, according Bjorken's formulae [20]:

$$\epsilon = \frac{3}{2} \frac{<p_T>}{\tau \pi R^2} \frac{dN}{d\eta} \qquad (2)$$

For Au-Au collisions at $\sqrt{s_{NN}} = 130$ and $\sqrt{s_{NN}} = 200$ the estimated energy densities are $3.6 GeV/Fm^3$ and $4.5 GeV/Fm^3$, respectively [6].

Therefore, for establishing the density energy in d-Au collisions at some considerations on momentum spectra and the inverse slope are needed. They are included in this paper. Before this, a short presentation of the results on participants is done.

5. Participants, momentum spectra and energy density in d-Au collisions

As it was mentioned previously, the total number of participant nucleons is an important physical quantity in the comparison with the model predictions. Establishing the participants' number information on the net baryon number, the number of pairs, as well as information on the energy density could be available.

Two ways are described in this paper. First of them consider the experimental results obtained in d-Au collisions at $\sqrt{s_{NN}} = 200$ [13, 21] and those obtained in full overlap d-Au collisions at $\sqrt{s_{NN}} = 19.4$ by the NA35 collaboration from CERN [22]. The second uses a geometrical model [23], corrected for relativistic nuclear collisions at colliders [24].

For estimating the participants' number has been taken into account the fact that, in lighter colliding systems, with a high collision asymmetry, the events selection for a given collision centrality, based on the impact parameter selection on the basis of a simulation code (HIJING, in previous experiment), is not longer possible. Therefore, a collision centrality selection based on the range of multiplicity has been used for d-Au collisions at $\sqrt{s_{NN}} = 200$. The forms of the pseudorapidity distributions, for different centrality ranges, confirm this.

An additional analysis was necessary to explore the potential bias that the different acceptances of the multiplicity array - formed by scintillation tiles and silicon detectors - could introduced on the experimental pseudorapidity distributions and, as a consequence, on the participants' number. The HIJING and GEANT simulation codes have been used. The most significant effects are observed for peripheral collisions (60-80% centrality cut) [25].

The connection between particle yields and centrality was analyzed using the experimental observation that the multiplicity of the charged particles correlates well to the impact parameter in the pseudorapidity range $-2.2 \leq \eta \leq 2.2$. In this analysis three collision centrality ranges have been considered, according to the multiplicity of each event, namely: 0%-20% (central events), 30%-50% (semicentral events) and 60%-80% (peripheral events). These multiplicities were scaled using the histograms for transverse momentum (Fig.6) [26].

The corresponding histograms for centrality ranges, namely: $N_{central}(p_T) = \frac{1}{N_{coll}}N_{0\%-20\%}$, $N_{semicentral}(p_T) = \frac{1}{N_{coll}}N_{30\%-50\%}$, $N_{peripheral}(p_T) = \frac{1}{N_{coll}}N_{60\%-80\%}$, permitted to obtain the number of participants. The results are included in Table I. These results are slightly higher than those obtained for the previous 0%-30%, 30%-60% and 60%-80% centrality ranges. The participants' numbers obtained for these ranges are: 13.6±0.3, 8.5±0.3, 4.7±0.3, respectively. All results are in reasonable agreements with some model calculations performed recently for number of participants, N_{part}, and for number of collisions, N_{coll} [17, 18, 27].

Scaled ratios central-to-peripheral and mid-central-to-peripheral for the number of participants are shown in Fig.7. These ratios were constructed for the centrality ranges 0%-30%, 30%-60% and 60%-80% as follows:
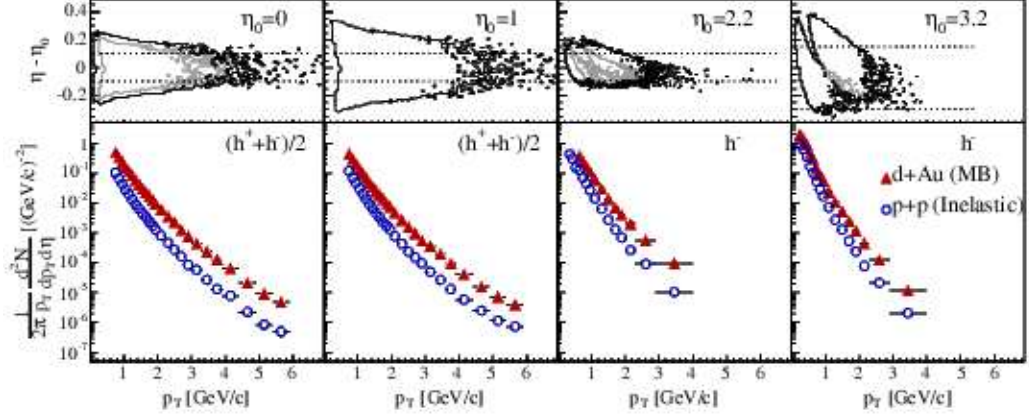
Fig. 6. Invariant yield distributions for charged hadrons produced in d-Au collisions and p-p collisions at $\sqrt{s_{NN}} = 200 GeV$ for 4 pseudorapidities, namely: $\eta = 0.0$, $\eta = 1.0$, $\eta = 2.2$ and $\eta = 3.2$

Table 1. Values for Npart and Ncoll obtained for d-Au at 200 AGeV

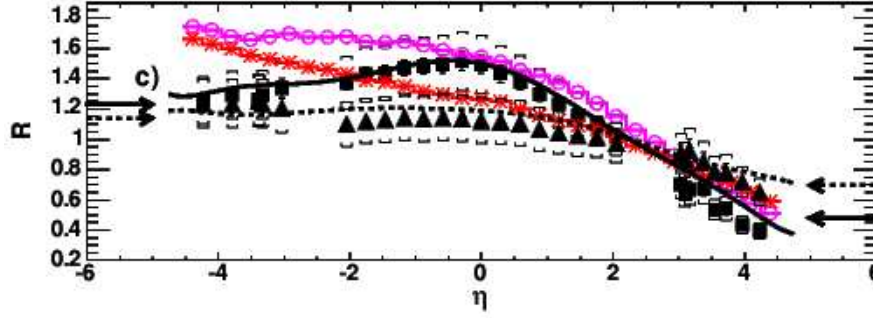| Centrality	$N_{part}(Au)$	$N_{part}(d)$	N_{coll}
0% − 20% (central events)	12.50	1.96	13.6±0.3
30% − 50% (semicentral events)	7.36	1.79	7.9±0.4
60% − 80% (peripheral events)	3.16	1.39	3.3±0.4

Fig. 7. Scaled ratios $R(0-30)\%$ (squares) and $R(60-80)\%$ (triangles) for d-Au collisions at $\sqrt{s_{NN}} = 200 GeV$

$$R^{(0-30)\%} = (0.35 \pm 0.03) \frac{\frac{dN^{(0-30)\%}}{d\eta}}{\frac{dN^{(60-80)\%}}{d\eta}} \tag{3}$$

$$R^{(30-60)\%} = (0.56 \pm 0.04) \frac{\frac{dN^{(30-60)\%}}{d\eta}}{\frac{dN^{(60-80)\%}}{d\eta}} \tag{4}$$

These scaled ratios have been compared with the HIJING simulation code predictions (curves in Fig.7). They describe well the experimental ratios. The unrestricted HIJING calculations (open circles and open asterisks) are included, too. They did not describe the experimental ratios, especially for the participants from gold. The systematic uncertainties for the ratios include the participant scaling uncertainty, as well as 5% uncertainty for the experimental pseudorapidity density ratios.

The experimental results were compared with similar experimental results obtained in d-Au collisions at CERN-SPS, at $\sqrt{s_{NN}} = 19.4$ [22]. This comparison suggests similar behaviour, in the deuteron fragmentation region, for d-Au collisions at the two mentioned energies [25]. The calculations based on the saturation picture, with parameters obtained from the experimental results for Au-Au collisions, did not reproduce results obtained in d-Au collisions at $\sqrt{s_{NN}} = 200$.

As was mentioned of the beginning of this part other way was tried too, for establishing the number of participants. Using the assumptions of the geometrical model [23, 24] the number of participant nucleons, as well as the time to travel one nucleus through the other were estimated. The obtained values for participant nucleons are slightly higher than those obtained experimentally. Using the weights for the different collision centrality ranges, as well as a better average for impact parameters, in agreement with those proposed in [27] and based on Glauber calculation of the nuclear overlap, the agreement with the experimental values increased. The

final values for the three collision centrality cuts are: 14.9 ± 0.8, 9.1 ± 0.9, 5.4 ± 0.8, respectively. Weights from HIJING simulation code have been used for the three collision centrality cuts. The time for the cessation of the contact between the two colliding nuclei is from 0.3 Fm/c - for the contraction at the initial stage, up to 1.9 Fm/c - for the final stage (no contact between colliding nuclei). These values of the time, the associated equivalent spherical radii, and the experimental values of the pseudorapidity density permitted to estimate the energy density in the range from 2,66 GeV/Fm^3 (most central collisions) to 0,42 GeV/Fm^3 (peripheral collisions). The values are significantly lower that those obtained in Au-Au collisions at the same energy, as well as at , 4.5 GeV/Fm^3 and 3.6 GeV/Fm^3, respectively.

6. Momentum spectra and high pT suppression

Usually, the high momentum particles are considered as a good probe to investigate the conditions prevailing early in the evolution of a system. Such particles can be associated with different production mechanisms like jet production; they can loss energy due to induced gluon radiation passing through a medium with a high density of color charges. As a consequence, a depletion of the high transverse momentum component can by observed in the spectra. Therefore, efforts to obtain new experimental results have been done [21, 26, 28–32].

In the attempt to evidence the gluon saturation in d-Au collisions at RHIC a study of the transverse momentum dependence on the nuclear modification factors, R_{dAu}, in function of collision centralities and of pseudorapidity, for produced hadrons, has been done [21, 26].

Taking into account the previous results included in this paper, four values of the pseudorapidity are considered: $\eta = 0.0$, $\eta = 1.0$, $\eta = 2.2$ and $\eta = 3.2$, respectively.

The experimental data have been collected with the both spectrometers and the INEL detectors, because of the high collision asymmetry and low multiplicity. INEL detectors have been used to select collision vertex. The criteria imposed for d-Au collisions and p-p collisions were related to the selection of the events with collision vertex within ±15 cm from the nominal collision vertex. The resolution imposed in the collision vertex determination was 5 cm.

In the obtaining of the momentum spectra of the charged hadrons similar methods as those presented previously have been used [33].

The invariant yields (in transverse momentum and pseudorapidity) of the charged hadrons, at the four mentioned pseudorapidities, are shown in Fig.6. For $\eta = 2.2$ and $\eta = 3.2$, respectively, only the invariant yields for negative hadrons are included. The spectra from the Fig.6 have been obtained using several magnetic fields settings. The results have been corrected for acceptances, trigger efficiency and tracking reconstruction efficiency. They were not corrected for weak decays and absorption. An overall systematic error of 15% is estimated and included in plots. The resolution in momentum is as described in chapter 3.

Table 2. Fit parameters for the power law function from eq.(5) in p-p and d-Au collisions at 200 AGeV

Collision	$\frac{(dN/d\eta)_{fit}}{(dN/d\eta)_{meas}}$	p_0	n	χ^2/NDF
$p-p$	$\frac{1.05\pm0.06}{0.95\pm0.07}$	1.18 ± 0.16	10.9 ± 0.9	$13.0/11$
$d-Au$	$\frac{2.23\pm0.09}{2.1\pm0.7}$	1.52 ± 0.10	12.3 ± 0.5	$10.2/11$

The plots include the dependence of the difference $\eta-\eta_0$ - with $\eta_0 = 0.0, 1.0, 2.2, 3.2$, respectively - on the transverse momentum. Gray lines show the overlaps among different magnet spectrometers settings.

For p-p collisions an additional correction for trigger efficiency was introduced. This correction take into account the difference between the measurements and the total inelastic cross section, in minimum bias mode. The trigger efficiency correction is $(135)\%$. It is important to stress that for p-p collisions the experimental data for forward angles have been collected, in majority, with magnet spectrometers settings to favour the negative particle detection.

The spectra for negative charged particles at the pseudorapidity $\eta = 3.2$ have been fitted with a power law function as follows:

$$\frac{1}{2\pi}\frac{d^2N}{p_T dp_T d\eta} \sim \frac{C}{(1+\frac{x}{p_0})^n} \tag{5}$$

where C is a fit constant, x is the fractional longitudinal momentum, and p_0 a fit parameter.

The integral of the that function over p_T^2 was compared with UA5 Experiment results [34], as well as with the results obtained in p-p and d-Au collisions at $\sqrt{s_{NN}} = 200$. The comparison results are included in Table II.

One of the most important parts of the study was the connection with the behaviour of the nuclear modification factor and the possibility to observe the high p_T suppression in d-Au collisions at the maximum RHIC energy. The p-p collisions have been used for comparisons taking into account the assumption that the production of moderately high transverse momentum particles scales with the number of binary collisions, N_{coll}, in the initial stages.

The nuclear modification factor for d-Au collisions is defined as follows:

$$R_{dAu} = \frac{1}{<N_{coll}>}\frac{N_{dAu}(p_T,\eta)}{N_{pp}(p_T,\eta)} \tag{6}$$

The values of the number of collisions in the initial stage are included in Table I. The average number of collisions for minimum bias was estimated as: $<N_{coll}> = 7.2 \pm 0.3$ in agreement with HIJING code simulations.

The dependences of the experimental nuclear modification factor, defined in Eq.(6), on the transverse momentum are presented in Fig.8, for the four pseudora-
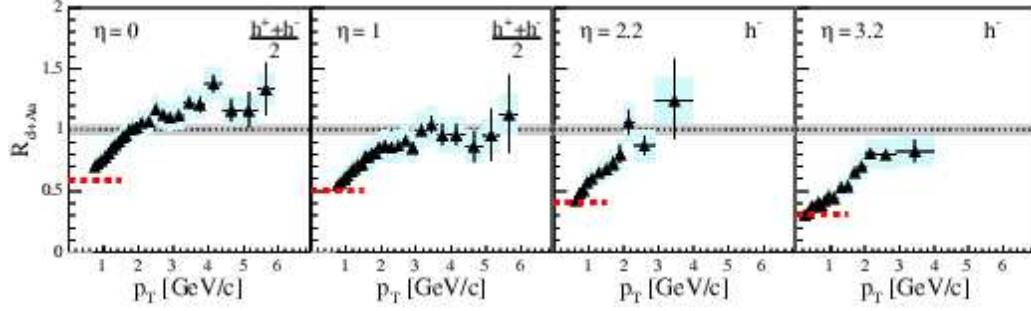
Fig. 8. Dependencies of the nuclear modification factor on the transverse momentum for charged hadrons in d-Au collisions at $\sqrt{s_{NN}} = 200 GeV$ for 4 pseudorapidities, namely: $\eta = 0.0$, $\eta = 1.0$, $\eta = 2.2$ and $\eta = 3.2$

pidities, namely: $\eta = 0.0$, $\eta = 1.0$, $\eta = 2.2$ and $\eta = 3.2$, respectively. Statistical errors are shown with error bars, and the systematic errors with shaded boxes with widths given by the bin sizes (are estimated around 15%). The error estimated for ratio because the normalization at the average number of collisions is represented, too (shaded band around unity). The normalized charged hadrons density ratio $\frac{1}{<N_{coll}>}\frac{(dN/d\eta)_{dAu}}{(dN/d\eta)_{pp}}$ is included, for $p_T < 1 GeV/c$ (dashed lines).

The results for two pseudorapidities - $\eta = 2.2$ and $\eta = 3.2$, respectively - are only for negative charged hadrons. This selection is motivated to the very low statistics for positive charged hadrons. In the other two plots, for pseudorapidities $\eta = 0.0$ and $\eta = 1.0$, respectively, the average charge $\frac{h^+ + h^-}{2}$ of the charged hadrons is used. This is useful because could compensate the difficulties related to the isospin symmetry.

At the pseudorapidity $\eta = 0.0$ the nuclear modification factor exceeds value 1, for $p_T > 2 GeV/c$. The behaviour is similar with those observed at lower energies [35]. The observed enhancement, in comparison with the binary collisions scale, has been considered as the effect of the multiple scattering at the partonic level [36]. Looking at the transverse momentum dependence of the same quantity for pseudorapidity $\eta = 1.0$, the disappearing of the enhancement due to Cronin effect is observed. The same behaviour is observed at the higher pseudorapidities, $\eta = 2.2$ and $\eta = 3.2$, respectively. Therefore, at the forward pseudorapidities the Cronin peak disappearing, for $p_T > 2 GeV/c$, could be affirmed. For the pseudorapidity the experimental results suggest suppression for all values of the transverse momentum.

For studying more the dependence on the collision centrality of the interesting physical quantities, the same method as for multiplicity was used. The central to peripheral and semi-central to peripheral ratios dependences on transverse momentum have been done, for d-Au collisions at $\sqrt{s_{NN}} = 200$. In Fig.9 the behaviour of the two ratios on the transverse momentum, for the four pseudorapidities, are
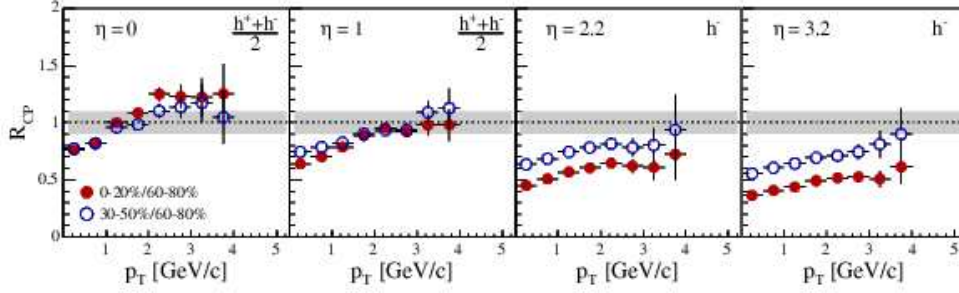
Fig. 9. Dependencies of the central to peripheral ratio and semicentral to peripheral ratio on transverse momentum in d-Au collisions at $\sqrt{s_{NN}} = 200 GeV$ for 4 pseudorapidities, namely: $\eta = 0.0$, $\eta = 1.0$, $\eta = 2.2$ and $\eta = 3.2$

shown. For $\eta = 0.0$ the central events yields (full circles) are systematic higher than the semicentral events (open circles), at $\eta = 1.0$ the two yields are almost equal, and for higher rapidities, $\eta = 2.2$ and $\eta = 3.2$, respectively, the situation changes: the semicentral events yields are higher than the central events yields. For example, at $\eta = 3.2$ the yields of central events are around 60% lower than the semicentral events, for all values of the transverse momentum.

An interesting result obtained at the forward pseudorapidity, $\eta = 3.2$, is presented in Fig.10. The spectra of the positive and negative charged hadrons present differences with the increasing of the transverse momentum. This type of behaviour could be related to de valence quark fragmentation [37]. Other explanation of this behaviour could be related to the string breaking mechanisms [38].

The studies included in this talk indicate that there is an evolution of the charged particle yields with the pseudorapidity, in comparison with mid-rapidity, to a gradual suppression to the forward pseudorapidities. The suppression increases with the collision centrality.

7. Final remarks

These results are related to the previous results obtained in Au-Au and d-Au collisions at RHIC-BNL energies. Many theoretical efforts in description of the experimental results obtained at RHIC have been done [39–42]. The hypotheses include different ways like partonic multiple collisions, collective flow and hydrodynamics, color glass condensate, perturbative QCD with different components, etc. Some of them give numerical simulations, too, for interesting physical quantities. There are some simulations that describe BRAHMS results. One of them is included in the collaboration papers (see references).

The experimental results presented in this talk indicate, using different ratios, that baryons and mesons have different behaviours according with its pseudorapid-
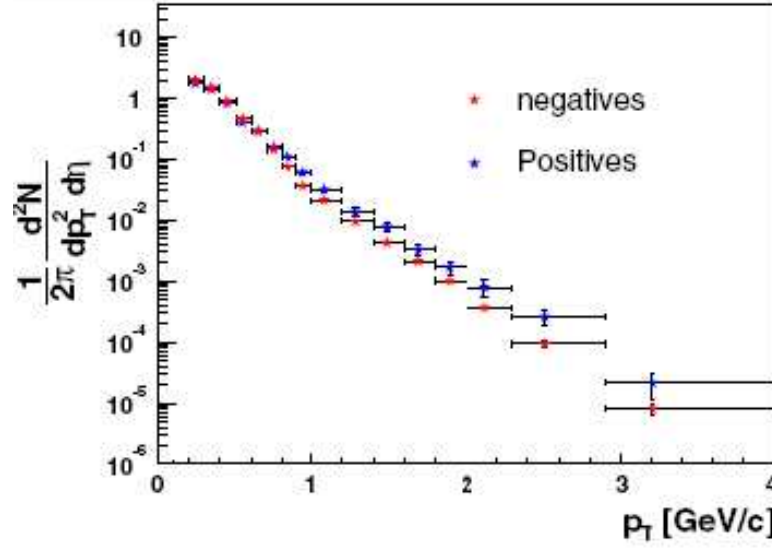
Fig. 10. Spectra of positive and negative charged particles produced in d-Au collisions at $\sqrt{s_{NN}} = 200 GeV$ for $\eta = 3.2$

ity. The composition of the produced hadrons changes with pseudorapidity, too. The new results of the BRAHMS Experiment, for d-Au collisions at different pseudorpaidities show that Physics at forward angles is a fertile ground for discovery. For qualitative improvement in tracking forward spectrum, trigger efficiency, centrality new data tacking at maximum RHIC-BNL energy is necessary.

The experimental results from obtained with BRAHMS detectors are consistent with formation of a hot and dense system that exhibits a high degree of reaction transparency leading to the formation of a near baryon free central region. There is a considerable energy loss of the colliding nuclei; therefore, conditions for the formation of a very high energy density zone with approximate balance between matter and antimatter in a rapidity interval from -1,5 up to 1,5, around mid-rapidity, are present. There are indications that the initial energy density is considerable large, so it is difficult to consider that the hadrons are isolated and well defined entities. Chemical equilibrium is suggested from the relative abundances of different particles. The temperature at equilibrium is around 175 MeV. Small chemical potential are observed.

General conditions for formation of a deconfined system of quarks and gluons appear, but other features defining the quark gluon plasma are absent or are not been identified up to now (for example, vanishing interactions between quarks, characteristics of the chiral symmetry restoration, clear phase transition behaviour of the system).

"There is not doubt that the experiments at RHIC have revealed a plethora of new phenomena for the most part have come a surprise. In this sense it is clear that the matter that is created at RHIC differs from anything that has been seen before. What name to give it must await our deeper understanding of this matter" [43].

Notes

a. Permanent address: Faculty of Physics, University of Bucharest, P.O.Box MG-11, RO 077125 Bucuresti-Magurele, ROMANIA
E-mail: jipa@brahms.fizica.unibuc.ro

References

1. D.Beavis et al - BRAHMS Conceptual Design Report, October 1994, BNL-62018
2. Fl.Videbaek - The BRAHMS Experiment at RHIC. Goals and Status - Workshop UIC, June 14-17, 1998, World Scientific, Singapore, 1999
3. F.Videbaek for the BRAHMS Collaboration "International Conference Quark Matter 2001" - Stony Brook and Brookhaven, January 2001, USA, invited lecture, published in Nuclear Physics A698(2002)29c-38c
4. Al.Jipa for the BRAHMS Collaboration, *Rom.Rep.Phys.* **53(3-8)** (2001) 323-334
5. M.Adamczyk et al (BRAHMS Collaboration), *Nucl.Inst.Meth.Phys.Res.* **A499** (2003) 437-468.
6. Al Jipa for the BRAHMS Collaboration, *Acta Physica Ungarica A: Heavy Ion Physics* **23** (2005)- in press
7. L.V.Gribov, E.M.Levin, M.G.Ryskin, *Phys.Rep.* **100** (1983) 1
8. D.Kharzeev, E.M.Levin, *Phys.Lett.* **B523** (2001) 79
9. B.B.Back et al (PHOBOS Collaboration), *Phys.Rev.Lett.* **85** (2000) 3100
10. C.Adler et al (STAR Collaboration), *Phys.Rev.Lett.* **87** (2001) 112303
11. K.Adcox et al (PHENIX Collaboration), *Phys.Rev.Lett.* **86** (2001) 3500
12. I.G.Bearden et al (BRAHMS Collaboration), *Phys.Rev.Lett.* **87** (2001) 112305
13. I.Arsene et al (BRAHMS Collaboration), Preprint nucl-ex/0401025
14. B.B.Back et al (PHOBOS Collaboration), accepted for publication in *Phys.Rev.Lett.* (2004) (Preprint nucl-ex/0311009)
15. X.N.Wang, M.Gyulassy, *Comput.Phys.Commun.* **83** (1994) 30, M.Gyulassy, Xian-Nian Wang, Preprint LBL, LBL-34246(2000)
16. AMPT Coll. (B.Zhang, C.M.Ko, B.A.Li, Z.Lin), *Phys.Rev.* **C61** (2000) 067901
17. D.Kharzeev, E.Levin, M.Nardi, *Nucl.Phys.* **A730** (2004) 448
18. D.Kharzeev, E.Levin, M.Nardi, *Nucl.Phys.* **A743** (2004) 329
19. I.G.Bearden et al (BRAHMS Collaboration), *Phys.Rev.Lett.* **88** (2002) 202301

20. J.D.Bjorken, *Phys.Rev.* **D27** (1983) 140
21. I.Arsene et al (BRAHMS Collaboration), *Phys.Rev.Lett.* **93** (2004) 242303
22. T.Alber et al, *Eur.Phys.J.* **C2** (1998) 643
23. Al.Jipa, *J.Phys.G: Nucl.Part.Phys.* **22** (1996) 231
24. Al.Jipa et al, *Rom.Rep.Phys.***52** (2000) 599
25. I.Arsene et al (BRAHMS Collaboration), *Phys.Rev.Lett.* **94** (2005) - in press
26. R.Debbe for the BRAHMS Collaboration, *J.Phys.G: Nucl.Part.Phys.* **30** (2004) S759-S765
27. R.Vogt, *Phys.Rev.* **C70** (2004) 064902
28. J.J.Gaardhoje for the BRAHMS Collaboration, *Nucl.Phys.* **A734** (2004) 13-27
29. C.E.Jorgensen for the BRAHMS Collaboration, *Nucl.Phys.* **A734** (2004) 65-69
30. Zhangbao Yin for the BRAHMS Collaboration, *J.Phys.G: Nucl.Part.Phys.* **30** (2004) S983-S987
31. K.Hagel for the BRAHMS Collaboration, Proceedings of the CCAST 2004, Beijing, China, in press
32. Al.Jipa for the BRAHMS Collaboration, Lecture given at The 4th Winter School on Relativistic Heavy Ion Collisions, Budapest, Hungary, December, 1-3, 2004
33. I.Arsene et al (BRAHMS Collaboration), *Phys.Rev.Lett.* **91** (2003) 072305
34. G.J.Alner et al, *Z.Phys.* **C33** (1986) 1
35. D.Antreasyan et al, *Phys.Rev.* **D19** (1979) 764
36. A.L.S. Angelis et al, *Nucl.Phys.* **B209** (1982) 209
37. M.Gyulassy, Proceedings of the RIKEN Workshop 2003, vol.57, p.141
38. S.Brodsky, F.Gunion, J.H.Kuhn, *Phys.Rev.Lett.* **39** (1977) 1120
39. R.C.Hwa, C.B.Yang, *Phys.Rev.* **C68** (2003) 024907
40. V.Guzey, M.Strikman, W.Vogelsang, *Phys.Lett.* **B603** (2004) 173
41. Ed.Iancu, K.Itakura, D.N.Triantafyllopoulos, *Nucl.Phys.* **A742** (2004) 182
42. M.Gyulassy, L.McLerran, *Nucl.Phys.* **A** (2005), in press
43. I.Arsene et al (BRAHMS Collaboration), *Nucl.Phys.* **A** (2005) - in press (BRAHMS white paper)